IOP Publishing Physica Scripta
Phys. Scr. 95 (2020) 105706 (8pp) https://doi.org/10.1088/1402-4896/abb736

Geometrical confinement effects on fundamental thermal properties of rutile and anatase TiO_2 cylindrical and tubular nanostructures

K Feddi[1,2], M Kria[3], M El-Yadri[3], F C Fobasso Mbognou[4], G Long[5], A Tiutiunnyk[6], L M Pérez[6], D Laroze[6,*] and E Feddi[3,*]

[1] EIMIS Laboratory, FST, University Abdelmalek Essadi, Tanger, Morocco
[2] Renewable Energy and Advanced Materials Laboratory, International University of Rabat, Morocco
[3] Group of Optoelectronic of Semiconductors and Nanomaterials, ENSET, Mohammed V University in Rabat, Morocco
[4] Mesoscopic and Multilayers Structures Laboratory, Department of Physics, Faculty of Science, University of Dschang, P.O. Box 479, Dschang, Cameroon
[5] Department of Physics, St. John's University, Jamaica, NY 11439, United States of America
[6] Instituto de Alta Investigación, CEDENNA, Universidad de Tarapacá, Casilla 7 D, Arica, Chile

E-mail: dlarozen@uta.cl and e.feddi@um5s.net.ma

Received 8 June 2020, revised 24 August 2020
Accepted for publication 10 September 2020
Published 23 September 2020

Abstract

In this work, we investigated the influence of the geometrical confinement effects on the fundamental thermal properties of rutile and anatase TiO_2 for both cylindrical nanostructures (CNSs) and nanotubular structures (NTSs), respectively. Calculations of energy levels are developed in the framework of effective mass approximation by generalizing the resolution of Schrödinger equation in a truncated cylinder. The energy spectrum is then used in the determination of thermodynamic properties by using the Boltzmann-Gibbs distribution. Numerical computations done for both rutile and anatase TiO_2 nanomaterials reveal a strong localization of the electron orbitals along to the lateral surface for all the studied are CNS and NTS. The average energy, heat capacity, entropy, and Helmholtz free energy calculated for different thicknesses for NTS and different cross-sections of CNS. Our numerical investigation shows that all thermodynamic properties depend on the temperature, the cross-section for the CNS, and the shell thickness for the NTS. We demonstrated that for low thickness, the heat capacity shows a Schottky-like anomaly at low temperatures. We also show that the Rutile structure is more stable than anatase. We hope that the thermodynamic properties concluded from this study can be considered as useful information for understanding the thermodynamic properties of TiO_2 nanofibers.

Keywords: Tubular nanostructures, Thermal properties, TiO2 materials

(Some figures may appear in colour only in the online journal)

1. Introduction

The nanotechnology defines the manipulation of atoms or molecules at the nanoscale. This concept offers the possibilities to miniature devices with enhanced performance [1]. In

* Author to whom any correspondence should be addressed.

 © 2020 IOP Publishing Ltd Printed in the UK

semiconductor physics, systems with reduced dimensionality have been widely studied and extensively manufactured. The originality of these nanomaterials is that the charge carriers are confined in one, two, or three dimensions, which leads to partial or full quantizations of energy levels. Due to these novel atom-like optoelectronic properties, the study of nanomaterials is a rapidly growing subject of both fundamental and practical interest [2–4]. Materials of controlled sizes and shape at the nanoscale are a prerequisite for many applications in fields such as optoelectronics, quantum information, photovoltaics, catalysis, and medicine, to mention a few [5]. Therefore, it makes sense to deepen the investigations of their physicochemical properties well both theoretically and experimentally, from the perspective of controlling their behaviors and their functionality for various technological applications.

In this continuous influx of development of Nanomaterials and because of its potential, nanometric forms of Titan dioxide have been elaborated by different methods [6–11]. Titan dioxide, TiO_2, is a metal oxide characterized by its great capacity for harvesting the light. It is a wide bandgap semiconductor ($E_g = 3.0$–3.2 eV) having interesting physicochemical properties such as strong photocatalytic activity, non-toxicity, high chemical stability, and also its high photoelectric conversion performance. For these reasons and its low cost, it is considered as an excellent candidate for many applications such as photocatalysis, solar energy conversion and many other applications[12–20].

Due to their direct pathway for rapid transport of photogenerated carriers, the one dimensional (1D) TiO_2 nanostructures such as nanotubes or nanowires have found their application in UV photodetector or dye-sensitized solar cell [21–23]. Numerous studies have been developed to prepare nanostructured TiO_2 materials with different morphologies, including quantum dots, nanofibers, nanotubes, nanorods, and nanosheets [4, 24, 25]. Among the first experimental realizations are due to Zwilling *et al* who synthesized the TiO_2 porous film by anodic oxidation of a titanium sheet at low voltage [26, 27]. However, the first fabrication of TiO_2 nanotube arrays in a hafnium acid electrolyte with heights up to 0.5mm was performed in 2001[28]. From Experimental point of view, the anodic oxidation is one of the simple and powerful chemical methods to obtain a well-arranged array of nanotubes perpendicular to the substrate. This process allows the control of the porosity, size, and height of the nanotubes. More recently, Siowwoon *et al* [29] have prepared Self-organized titanium dioxide nanotube layers prepared by electrochemical anodization and applied them as the sensing layer in the photodetector as it is shown in figure 1. In fact, TiO_2 nanotube layers have attracted much attention due to the ease of preparation yet economical. For more details, we refer the reader to some references exploring the last achievement and applications of these nanostructures[30–35].

Generally speaking, the key factor limiting the performance of the solar cell is the competition between the flow of electrons and the interfacial electron-hole recombination. This phenomenon reduces the mobility of electrons and affects their collection at the back collector. This effect leads to the

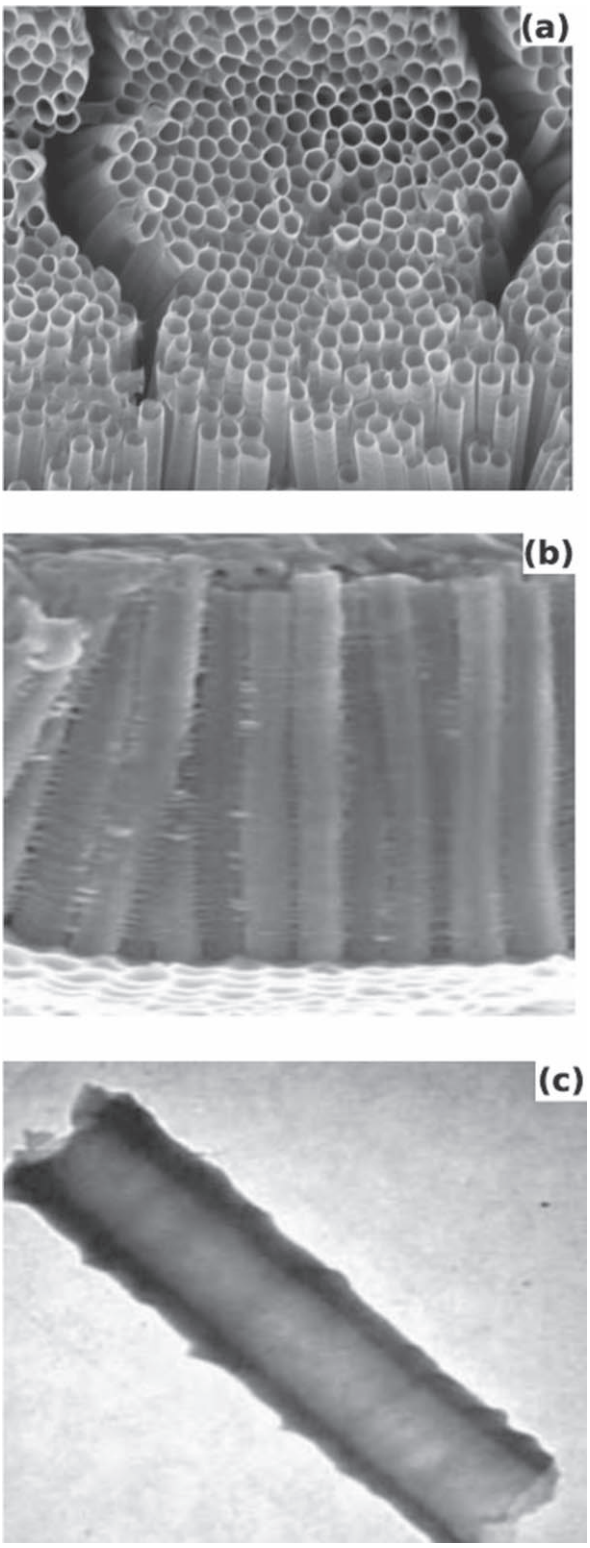


Figure 1. (a) SEM morphology of TiO_2 nanotubes. (b) Cross-sectional view morphology of TiO_2 nanotubes. (c) TEM image of single nanotube. We remark that the panel (a) was provided by Dr. Siow Woon (Brno University of Technology), and it has not published before. Panels (b) and (c) are taken from [29], with permission of the corresponding author and Elsevier.

weakness of the efficiency of solar energy conversion [18]. However in nanotubular TiO_2 , the existence of longitudinal pathways facilitates the extraction of charges between interfaces [36–38]. The oriented vertically tubular structures of TiO_2 induce an increase of the electron mobility along the vertical direction, which reduces the interface recombinations. Besides, Their high surface-to-volume ratio allows an important light scattering effect. For all these exceptional physical behaviors, the tubular nanostructures are considered potential candidates for solar energy harvesting.

We would like to emphasize that our analysis of the literature shows that to date, there has been no study concerning the influence of the thickness and the cross-section size effect on the fundamental thermodynamic properties of rutile and anatase TiO_2 for both cylindrical nanostructures (CNSs) and nanotubular structures (NTSs). To prove the stability of different crystallization phases of TiO_2, multiple experimental studies have focused on the heat capacity and thermodynamic functions of these compounds in different forms: bulk and nanowires. For more details, can be found in [39, 40]. Experimental measurements have shown that the rutile phase is generally less stable than anatase when the sizes of TiO_2 particles have almost 14nm. It has been also demonstrated that in bulk case, the Anatase structure is more stable, whereas The rutile structure is the stable bulk phase under high temperature and pressure [41–44]. More recently, Feng *et al* have initiated an experimental study on thermodynamic properties of TiO_2(B) nanowires with 50 nm in diameter and several micrometers in length. In particular, it has been observed that entropy of TiO_2(B) is found to be similar to brookite, but significantly higher than those of anatase and rutile when temperature is above 200 K [39].

The purpose of this paper is to determine the heat capacity, entropy, and Helmholtz free energy (NTS). We consider that our structure is immersed in a wide band dielectric medium such as curable resin or another polymer with a large gap considered as an infinity wall, which allows us to consider that charge carriers are confined in TiO_2 region. Calculations of energy levels will be performed in the framework of effective mass approximation by solving Schrödinger equation and considering the boundary conditions. The thermodynamic properties are determined by using the Boltzmann-Gibbs distribution. The manuscript is structured as follows: in section 2, we describe the essential features of our theoretical approach. Section 3 is devoted to numerical results and discussions. Finally, the conclusion and some perspectives are outlined in section 4.

2. Theoretical model

In this section, we present the theoretical model for the thermal properties of nano-tubular array. Let us present in figure 2 a pictorial view and the band offset of NTS. The thickness of a single NTS is defined by $L_w = R_s - R_c$, where R_c and R_s are the internal and external radii respectively. We suppose that our structure is immersed in the host matrix with

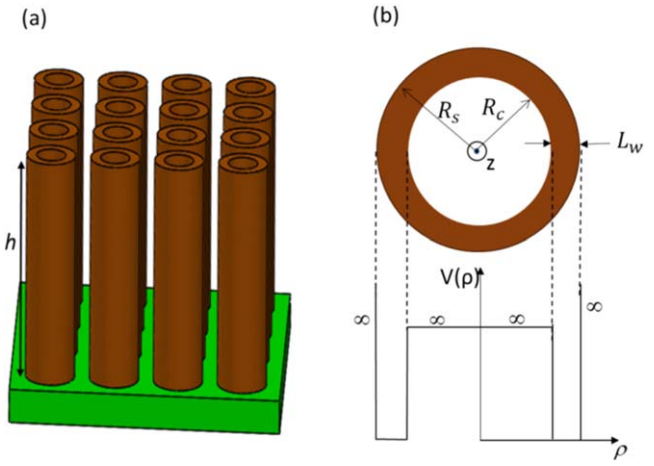


Figure 2. (a) Schematic view of the nano-tubular array structures used in the present study. (b) Band offsets representation of the lateral confinement, where R_c and R_s are the radii of core and shell materials, respectively, and $L_w = R_s - R_c$ is the well thickness.

a large bandgap, which allows us to consider that charge carriers are confined in TiO_2 region.

In the Boltzmann-Gibbs distribution, all fundamental thermodynamic properties can be investigated using the canonical partition function Z_c which involves all energy levels E_i obtained by the resolution of the Schrödinger equation $\mathcal{H}|i\rangle = E_i|i\rangle$ where $\mathcal{H}$ is the Hamiltonian of the system. The partition function is given by:

$$Z_c = \sum_i e^{-\beta E_i}, \tag{1}$$

where $\beta = 1/k_B T$, k_B is the Boltzmann constant, T is the temperature expressed in Kelvin. Taking into account that the volume is constant, the average energy of the system is calculated through the relation

$$\langle E \rangle = -\frac{\partial \ln Z_c}{\partial \beta}. \tag{2}$$

The different thermodynamic properties of the system are calculated using the partition function Z_c. We note that the heat capacity of the system which informs us about the storage energy in nanostructure is given by:

$$C_V = -k_B \beta^2 \left(\frac{\partial \langle E \rangle}{\partial \beta} \right) \tag{3}$$

One the of most important thermodynamic property is the entropy, which gives an idea about the randomness in the system. It is given by:

$$S = k_B \beta (\langle E \rangle - F_H), \tag{4}$$

where $F_H = -\beta^{-1} \ln Z_c$ is the Helmholtz free energy used usually as a criterion of stability.

On the other hand, in the frame work of the effective mass approach, the Hamiltonian of one electron can be

written as:

$$\mathcal{H}(\rho_e, \varphi_e, z_e) = -\frac{\hbar^2}{2m_e^*}\Delta_e(\rho_e, \varphi_e, z_e) + V_w^e(\rho_e) + V_w^e(z_e) \tag{5}$$

where

$$\Delta_e(\rho_e, \varphi_e, z_e) = \left(\frac{\partial^2}{\partial\rho_e^2} + \frac{1}{\rho_e}\frac{\partial}{\partial\rho_e} + \frac{1}{\rho_e^2}\frac{\partial^2}{\partial\varphi_e^2} + \frac{\partial^2}{\partial z_e^2}\right)$$

is a Laplacian in cylindrical coordinates, m_e^* is the effective mass of the electron, and $V_w^e(\rho_e)$ and $V_w^e(z_e)$ are the confinement potentials, respectively. These potential are explicitly given by [45]:

$$V_w^e(\rho_e) = \begin{cases} 0 & \text{for} \quad R_c \leqslant \rho_e \leqslant R_s \\ \infty & ; \quad \text{otherwise} \end{cases};$$
$$V_w^e(z_e) = \begin{cases} 0 & \text{for} \quad |z_e| \leqslant h/2 \\ \infty & ; \quad \text{otherwise} \end{cases} \tag{6}$$

The energy and the wave function are given by the resolution of Schrödinger equation

$$\mathcal{H}\Psi_e(\rho_e, z_e, \varphi_e) = E_e\Psi_e(\rho_e, z_e, \varphi_e), \tag{7}$$

such that the wave function can be written as a product of the two independent parts:

$$\Psi_e(\rho_e, z_e, \varphi_e) = R_e(\rho_e)g_e(z_e)\exp(im\varphi_e) \tag{8}$$

Therefore, the radial wave function, R_e, can be obtained from the following equation

$$-\frac{\hbar^2}{2m_e^*}\left(\frac{\partial^2}{\partial\rho_e^2} + \frac{1}{\rho_e}\frac{\partial}{\partial\rho_e} - \frac{m^2}{\rho_e^2} + \frac{\partial^2}{\partial z_e^2}\right)R_e(\rho_e) + V_w^e(\rho_e)R_e(\rho_e) = E_{mn}R_e(\rho_e) \tag{9}$$

The exact solution for R_e is given by a linear combination of Bessel functions $J_m(k_{mn}\,\rho_e)$ and $Y_m(k_{mn}\,\rho_e)$ of first and second kind, respectively [46]:

$$R_e(\rho_e) = A_1\,J_m(k_{mn}\,\rho_e) + A_2\,Y_m(k_{mn}\,\rho_e) \tag{10}$$

where A_1 and A_2 are normalization constants obtained by boundary and normalization conditions of the wave functions, m is the order of Bessel functions. Indeed the radial wave function must vanish at the inner ($\rho_e = R_c$) and outer ($\rho_e = R_s$) radial borders as well as at the top and bottom of the cylinder. These conditions lead to the transcendental equation:

$$|J_m(k_{mn}\,R_c)Y_m(k_{mn}\,R_s) - Y_m(k_{mn}\,R_c)J_m(k_{mn}\,R_s)| = 0 \tag{11}$$

where k_{mn} is the n^{th} root of Bessel functions $J_m(k_{mn}\,\rho_e)$ and $Y_m(k_{mn}\,\rho_e)$. It means the number n characterize the set of all the roots of the Bessel functions. Therefore, the radial eigenenergies corresponding to the equation (9) are given by the equality $k_{mn}^2 = E_{mn}$.

On the other hand, in the z-direction, the corresponding Schrödinger equation is the standard problem of an infinite square well:

$$-\frac{\hbar^2}{2m_e^*}\frac{\partial^2}{\partial z_e^2}g_e(z_e) + V_w^e(z_e)g_e(z_e) = E_l g_e(z_e), \tag{12}$$

and its odd solution is:

$$g_e(z_e) = \sin\left(\frac{l\,\pi\,z_e}{h} + \frac{l\,\pi}{2}\right). \tag{13}$$

Then, the energy eigenvalues in z-direction is $E_l = (l\pi/h)^2$. Consequently, the total expression of the eigenenergies is given by the relation:

$$E_{nlm}^e = k_{mn}^2 + \left(\frac{l\pi}{h}\right)^2, \tag{14}$$

where $l = 1, 2,\ldots; m = 0, \pm1, \pm2, \ldots$.

Table 1. Physical parameters of anatase and rutile TiO_2 [47–51].

	m_e^*/m_0	ε	E_g (eV)	a^* (nm)	R^* (meV)
anatase	0.1412	31	3.2	11.63	1.99
rutile	0.1284	63.7	3	26.29	0.43

3. Results and discussion

In this section, the numerical computations will be performed for both rutile and anatase TiO_2 NTSs. The physical parameters of these two phases are listed in table 1. To evaluate how the shape and the crystallographic structure affect the thermodynamic properties of TiO_2, we must inspect the effects of two types of confinement in the two structures. We note that the size of lateral confinement defined by the outer radius R_s is called 3D confinement, while the confinement domain represented by the shell (well) defined by the thickness $L_w = R_s - R_c$ will be called 2D confinement. Foremost, to illustrate the charge distribution we show in figure 3 the fundamental and first excited state probability density amplitudes corresponding to anatase TiO_2 for an outer radius $R_s = 1a^*(11.63\,\text{nm})$ and an height $h = 10\,a^*(116\,\text{nm})$. In our study, we examine three well thicknesses corresponding to three values of the inner radius $R_c = 0$ ($L_w = 1\,a^*$), which is equivalent to a (CNS) of radius R_s, $R_c = 5\,\text{nm}$ ($L_w = 6.63\,\text{nm}$) and $R_c = 7\,\text{nm}$ ($L_w = 4.63\,\text{nm}$), the last two cases correspond to the NTSs.

The density representations show a strong localization of the electron orbitals along to the lateral surface for all structures. The electronic densities for the first excited, twice degenerate, it is more localized in the center with a regular distribution in the cylinder's internal space. For very thin values of L_w and a large value of R_s, the nanofiber is similar to a curved surface having only a few atomic layers so-called 2D materials. Our numerical calculation is performed for the number of successive states N from which the partition function becomes constant. Indeed, at $T = 100\,\text{K}$, Z_c saturates at $N = 5$ for anatase TiO_2, and it saturates at $N = 10$ for rutile TiO_2 for all the well thickness values computed. At $T = 300$

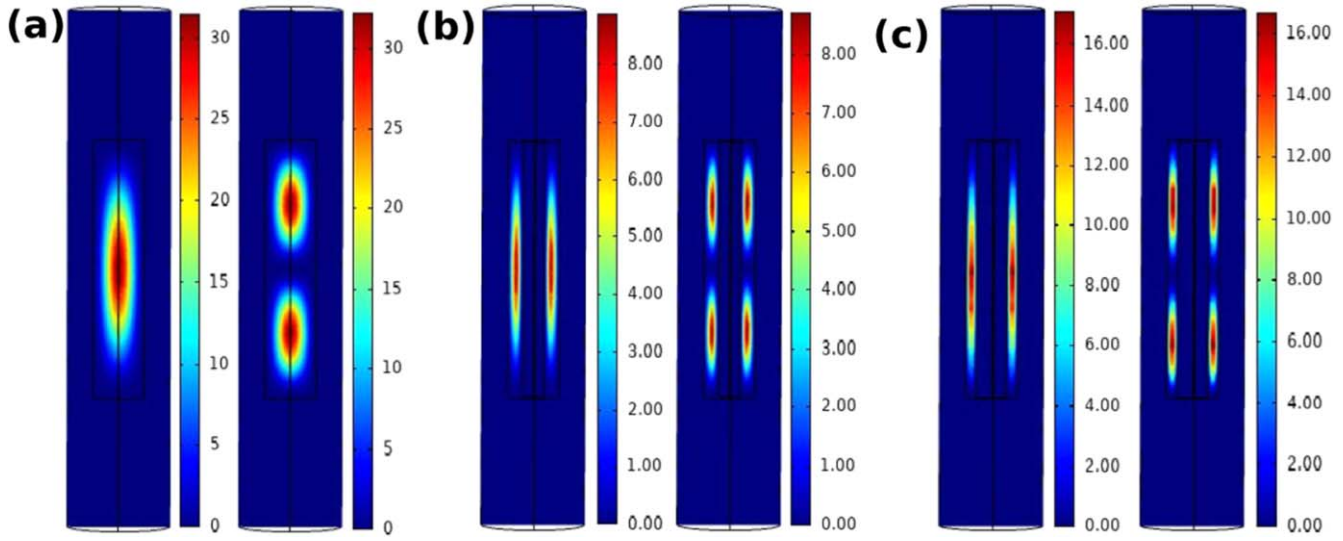


Figure 3. Probability densities of the lowest confined states in anatase TiO_2 nanotubular structures for $R_s = 11.63$ nm , $h = 116$ nm , and different values of core raduis: (a) $R_c = 0$ (b) $R_c = 5$ nm , (c) $R_c = 7$ nm.

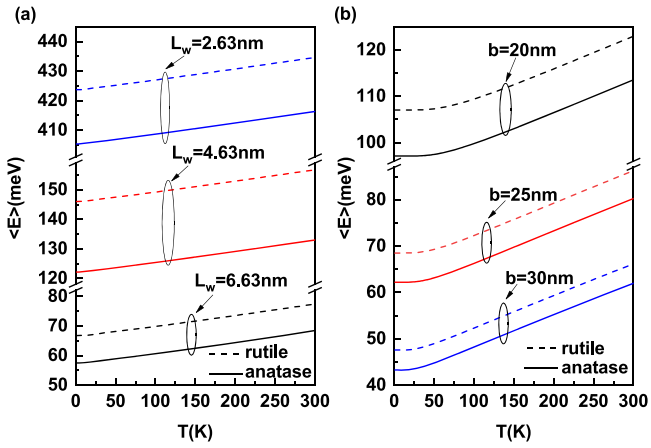


Figure 4. Average energies versus temperature of TiO_2 for NTS (a) and CNS (b).

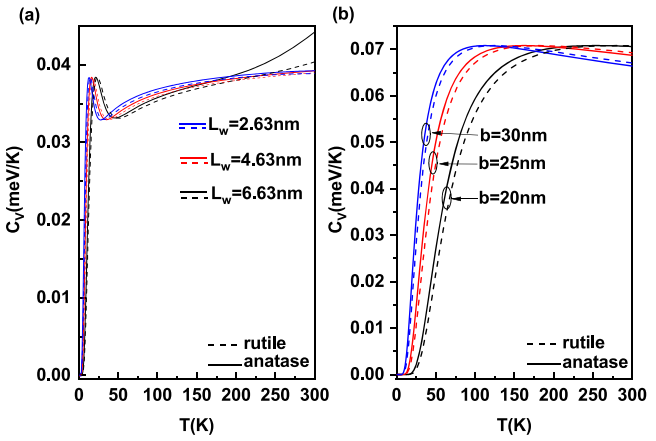


Figure 5. Heat capacity versus temperature of TiO_2 for NTS (a) and CNS (b).

K, we noticed that for $L_w = 2.63$ nm, the partition function saturated at $N = 15$ for both anatase and rutile forms However, for $L_w = 4.63$ nm, the saturation is obtained at $N = 25$ and $N = 20$ for the anatase and rutile, respectively. Finally, for $L_w = 6.63$ nm, Z_c saturates at $N = 30$ for anatase TiO_2 and at $N = 20$ for rutile TiO_2.

The partition function is used to compute the average energy values as a function of the temperature and the well-thickness for both cylindrical nanostructures as well as nanotubular structures. Panels (a) and (b) of figure 4 show that the average energies increase linearly for both anatase and rutile for CNS and NTS when increasing the temperature. They also show that the average energy is decreasing while increasing the well-thickness for a fixed temperature in the NTS case. As we analyze the evolution of the average energy as a function of the temperature in the rutile and anatase TiO_2 CNS, we note that the average energy remains constant at the lowest temperatures but starts rising at temperatures superior to $T = 50$ K. When we exceed this temperature, the average energy evolution is linear as a function of the temperature for a fixed outer radius. We also remark that the average energy value is more critical for the rutile TiO_2 for NTS (Figure 4(a)) and CNS (figure 4(b)) whatever the value of the temperature.

Figure 5 displays the evolution of heat capacity C_v as a function of temperature for rutile and anatase TiO_2, in the case of CNS and NTS, respectively. The heat capacity values were computed for three well-thickness for the NTS and three outer radii for CNS. Figure 5(a), shows the variation of the heat capacity C_v as a function of the temperature for both rutile and anatase TiO_2 in the case of the NTS. We notice that for a fixed well thickness, at low temperature, the heat capacity quickly peaks before starting a descent to a value from where it slightly increases until reaching a stabilization value. We also remark that for the lower temperatures below the peak value, as the well-thickness increases, the specific heat decreases. As it was interpreted by several authors [52–54], the peak in C_v in low dimension structures is not explained is similar to Schottky anomaly encountered in the heat capacity of two-level systems at low temperature. As we exceed the peak value and at higher temperatures, the heat

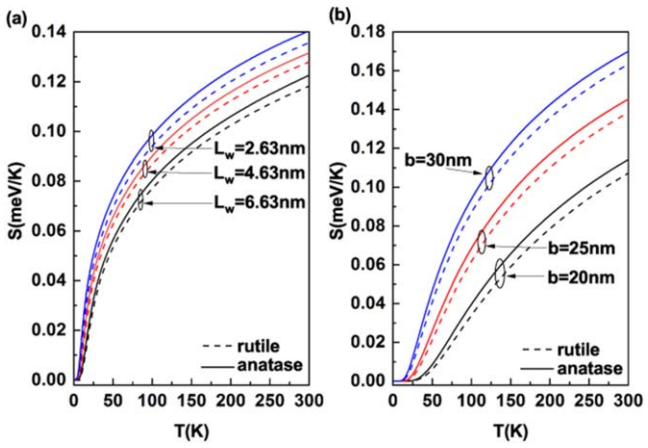


Figure 6. Entropy versus temperature of TiO_2 for NTS (a) and CNS (b).

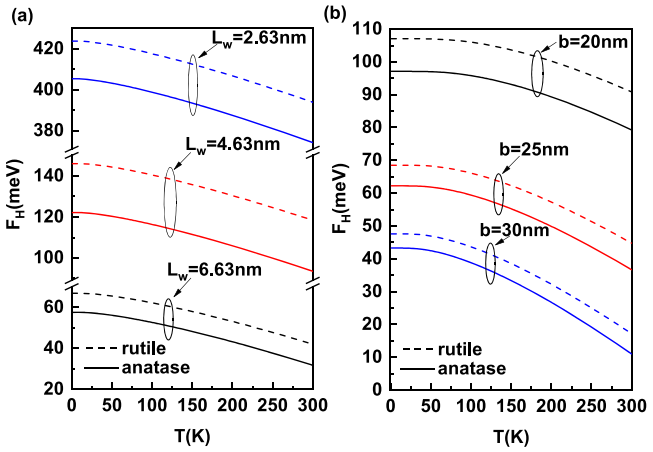


Figure 7. Helmholtz free energy versus temperature of TiO_2 for NTS (a) and CNS (b).

capacity for the most significant well thickness value exceeds others for both rutile and anatase. While examining the CNS heat capacity curves, one can observe for anatase at a fixed outer radius that the heat capacity reaches seemingly the same maximum value before it entering a slow and minimal descent than stabilization. We also notice that as the outer radius increases, the specific heat increases for low temperatures. This behavior is reversed at higher temperatures, as the heat capacity stabilizes, the external radius value increases, the heat capacity decreases. However, in the case of CNS, the heat capacity reaches values above to those observed in the NTS.

Figure 6 presents the variation of the entropy S as a function of the temperature for both rutile and anatase TiO_2, and in both configurations: cylindrical nanostructures as well as nanotubular structures. We observe that the entropy grows as the temperature increases for all settings. At very low temperatures, this property is tending to zero as it should, since the entropy determines the disorder of a system. However, we notice that the entropy is growing faster even for temperatures lower than 25 K, in the case of NTS for both anatase and rutile TiO_2 (figure 6(a)). At a fixed temperature, we notice that the entropy grows as we increase the well-thickness of NTS. On the other hand, for both anatase and rutile TiO_2 (figure 6(b)), for the CNS where the entropy remains a null value until it reaches 25 K. We remark that for fixed temperatures, the entropy increases when the outer radius increases for the CNS. We also note, that for the same temperature, and a fixed outer radius, the entropy in the anatase TiO_2 is superior to the entropy in rutile TiO_2, for both CNS and NTS, as well. Let us remark that our findings are in good agreement of the experimental values obtained by Feng *et al* [39].

Finally, to study the stability or both cylindrical nanostructures and nanotubular structures in the case of rutile and anatase TiO_2, figure 7 shows the Helmholtz free energy F_H as a function of temperature. In particular, different values of well-thickness (for NTS) and different values of the outer radiuses (for CNS) have been taken into account. We notice that for both NTS and CNS, the Helmholtz free energy decreases as the temperature grows. In the case of NTS at the same temperature, we remark that the Helmholtz free energy increases as the value of the well-thickness decreases for both anatase and rutile TiO_2, as it is shown in the panels (a) and (b) of figure 7, respectively. It is equivalent in the case of CNS, in which the value of Helmholtz free energy grows as the outer radius decreases for both anatase and rutile TiO_2. In general, for fixed temperature and core and outer radius, we remark that the Helmholtz free energy of the NTS for both rutile and anatase exceeds the Helmholtz free energy of the CNS.

4. Conclusions

We have evaluated the impact of thickness and size on the main thermodynamic properties of TiO_2 rutile and anatase cylindrical and tubular nanostructures. Within the framework of the effective mass approximation, we solve the Schrödinger equation analytically in two bands models, and we determine the energies of all excited states. By using the Boltzman-Gibbs distribution, energy states are used to evaluate the thermodynamic prosperities. Numerical computations done for both rutile and anatase TiO2 nanomaterials reveal a strong localization of the electron orbitals along to the lateral surface for all the studied structures CNS and NTS. The average energy, heat capacity, entropy, and Helmholtz free energy were calculated for different thicknesses for NTS and several cross-sections of CNS. Our numerical investigation shows that all thermodynamic properties depend on the temperature, the cross-section for the CNS, and the shell thickness for the NTS. We demonstrate that for low thickness, the heat capacity shows a Schottky-like anomaly at low temperatures. We also show that the Rutile structure is more stable than anatase. The thermodynamic properties concluded from this study can be considered useful for understanding the thermodynamic properties of TiO_2 nanofibers.

Acknowledgments

We sincerely thank Dr. Siow Woon Ng (Brno University of Technology, CEITEC, Czech Republic) for her useful discussions and for her permission to use the images of figure 1. Also, we thanks Prof. J. L. Bretonnet (Université de Lorraine, France) for his scientific support. AT acknowledges the financial support from Postdoctoral Fellowship FONDECYT 3 180 276. LMP and DL acknowledge partial financial support from FONDECYT 1 180 905. DL acknowledges partial financial support from Centers of excellence with BASAL/ANID financing, AFB180001, CEDENNA.

ORCID iDs

G Long https://orcid.org/0000-0002-4144-1879
A Tiutiunnyk https://orcid.org/0000-0003-1692-5561
L M Pérez https://orcid.org/0000-0002-2915-309X
D Laroze https://orcid.org/0000-0002-6487-8096
E Feddi https://orcid.org/0000-0001-6641-3623

References

[1] Feynman R P 1959 Plenty of room at the bottom *APS Annual Meeting of Physical Society atthe California Institute of Technology (Caltech), Caltech Engineering and Science* **23** 22–36 http://calteches.library.caltech.edu/1976/
[2] Loss D and DiVincenzo D P 1998 *Phys. Rev.* A **57** 120
[3] Sherwin M S, Imamoglu A and Montroy T 1999 *Phys. Rev.* A **60** 3508
[4] Michler P, Kiraz A, Becher C, Schoenfeld W, Petroff P, Zhang L, Hu E and Imamoglu A 2000 *Science* **290** 2282–5
[5] Tartakovskii A 2012 *Quantum Dots: Optics, Electron Transport and Future Applications* (Cambridge: Cambridge University Press)
[6] Uzer E, Kumar P, Kisslinger R, Kar P, Thakur U K, Zeng S, Shankar K and Nilges T 2019 *ACS Applied Nano Materials* **2** 3358–67
[7] Manique M C 2019 TiO2 nanotubes as photocatalyst for biodiesel production *Nanomaterials for Eco-friendly Applications* (Berlin: Springer) pp 49–66
[8] Mohammed N M, Bashiri R, Sufian S, Kait C F and Majidai S 2018 *Titanium Dioxide: Material for a Sustainable Environment, Intechopen* ed D. Yang 978-1-78923-327-8 (https://doi.org/10.5772/intechopen.70290)
[9] Bimberg D, Grundmann M and Ledentsov N N 1999 *Quantum dot Heterostructures* (New York: Wiley)
[10] Huffaker D, Park G, Zou Z, Shchekin O and Deppe D 1998 *Appl. Phys. Lett.* **73** 2564–6
[11] Anscombe N 2007 *Nat. Photonics* **1** 360–1
[12] Jiang Z, Yang F, Luo N, Chu B T, Sun D, Shi H, Xiao T and Edwards P P 2008 *Chem. Commun.* **47** 6372–4
[13] Yang L, Luo S, Liu R, Cai Q, Xiao Y, Liu S, Su F and Wen L 2010 *The Journal of Physical Chemistry* C **114** 4783–9
[14] Zhao J, Sallard S, Smarsly B M, Gross S, Bertino M, Boissière C, Chen H and Shi J 2010 *J. Mater. Chem.* **20** 2831–9
[15] Kim T W, Ha H W, Paek M J, Hyun S H, Choy J H and Hwang S J 2010 *J. Mater. Chem.* **20** 3238–45
[16] Etacheri V, Seery M K, Hinder S J and Pillai S C 2010 *Chem. Mater.* **22** 3843–53
[17] Yang G, Jiang Z, Shi H, Xiao T and Yan Z 2010 *J. Mater. Chem.* **20** 5301–9
[18] Zhu K, Neale N R, Miedaner A and Frank A J 2007 *Nano Lett.* **7** 69–74
[19] Kang T S, Smith A P, Taylor B E and Durstock M F 2009 *Nano Lett.* **9** 601–6
[20] Sauvage F, Di Fonzo F, Li Bassi A, Casari C S, Russo V, Divitini G, Ducati C, Bottani C E, Comte P and Graetzel M 2010 *Nano Lett.* **10** 2562–7
[21] Bach U, Lupo D, Comte P, Moser J E, Weissörtel F, Salbeck J, Spreitzer H and Grätzel M 1998 *Nature* **395** 583–5
[22] Feldt S M, Gibson E A, Gabrielsson E, Sun L, Boschloo G and Hagfeldt A 2010 JACS **132** 16714–24
[23] Grätzel M 2001 *Nature* **414** 338–44
[24] Qiu J, Yu W, Gao X and Li X 2006 *Nanotechnology* **17** 4695
[25] Formo E, Lee E, Campbell D and Xia Y 2008 *Nano Lett.* **8** 668–72
[26] Zwilling V, Darque-Ceretti E, Boutry-Forveille A, David D, Perrin M Y and Aucouturier M 1999 *Surf. Interface Anal.* **27** 629–37
[27] Zwilling V, Aucouturier M and Darque-Ceretti E 1999 *Electrochim. Acta* **45** 921–9
[28] Gong D, Grimes C A, Varghese O K, Hu W, Singh R, Chen Z and Dickey E C 2001 *J. Mater. Res.* **16** 3331–4
[29] Ng S, Yam F K, Sohimee S N, Beh K P, Tneh S S, Cheong Y L and Hassan Z 2018 *Sens. Actuators, A* **279** 263–71
[30] Mor G K, Varghese O K, Paulose M, Shankar K and Grimes C A 2006 *Sol. Energy Mater. Sol. Cells* **90** 2011–75
[31] Shankar K, Basham J I, Allam N K, Varghese O K, Mor G K, Feng X, Paulose M, Seabold J A, Choi K S and Grimes C A 2009 *The Journal of Physical Chemistry* C **113** 6327–59
[32] Ghicov A and Schmuki P 2009 *Chem. Commun.* 2791–808
[33] Roy P, Kim D, Lee K, Spiecker E and Schmuki P 2010 *Nanoscale* **2** 45–59
[34] Rani S, Roy S C, Paulose M, Varghese O K, Mor G K, Kim S, Yoriya S, LaTempa T J and Grimes C 2010 *Phys. Chem. Chem. Phys.* **12** 2780–800
[35] Yan J and Zhou F 2011 *J. Mater. Chem.* **21** 9406–18
[36] Pagliaro M, Palmisano G, Ciriminna R and Loddo V 2009 *Energy & Environmental Science* **2** 838–44
[37] Kongkanand A, Tvrdy K, Takechi K, Kuno M and Kamat P V 2008 JACS **130** 4007–15
[38] Baker D R and Kamat P V 2009 *Adv. Funct. Mater.* **19** 805–11
[39] Feng T, Li L, Shi Q, Che X, Xu X and Li G 2018 *The Journal of Chemical Thermodynamics* **119** 127–34
[40] JSmith S, Stevens R, Liu H, navrotsky A, Goates J B and Woodfield B F 2009 *Am. Mineral.* **94** 236–43
[41] Navrotsky A 2003 *Geochem. Trans.* **4** 34–7
[42] Gribb A and Banfield J 1997 *Am. Mineral.* **82** 717–28
[43] Zhang H and Banfield J 1998 *J. Mater. Chem.* **8** 22073–6
[44] SLevchenko A, Li G, Boerio-Goates J, Woodfield B and Navrotsky A 2006 *Chem. Mater.* **18** 6324–32
[45] Oukerroum A, Feddi E, Bailach J B, Martínez-Pastor J, Dujardin F and Assaid E 2010 *J. Phys. Condens. Matter* **22** 375301
[46] El-Yadri M, Feddi E, Aghoutane N, El Aouami A, Radu A, Dujardin F, Nguyen C V, Phuc H V and Duque C 2018 *J. Appl. Phys.* **124** 144303
[47] Zhang J, Zhou P, Liu J and Yu J 2014 *Phys. Chem. Chem. Phys.* **16** 20382–6
[48] Tang H, Prasad K, Sanjines R, Schmid P and Levy F 1994 *J. Appl. Phys.* **75** 2042–7
[49] Wypych A, Bobowska I, Traczd M, Opasinska A, Kadlubowski S, Krzywania-Kaliszewska A, Grobelny J and Wojciechowski P 2014 *J. Nanomater.* **2014** 124814
[50] Das S, Zazpe R, Prikryl J, Knotek P, Krbal M, Sopha H, Podzemna V and Macak J M 2016 *Electrochim. Acta* **213** 452–9

[51] Zhang J, Zhou P, Liub J and Yu J 2014 *Phys. Chem. Chem. Phys.* **16** 20382
[52] Boyacioglu B and Chatterjee A 2012 *J. Appl. Phys.* **112** 083514
[53] Baghdasaryan D, Hayrapetyan D, Kazaryan E and Sarkisyan H 2018 *Physica E* **101** 1–4
[54] Khordad R and Sedehi H R 2018 *J. Low Temp. Phys.* **190** 200–12